Experimental Investigation on Effects of Elastic Agitator to Turbulence Enhancement

T. H. Yong[1], H. B. Chan[1], S. S. Dol[2†], S. K. Wee[3] and S. A. Sulaiman[4]

[1]*Department of Mechanical Engineering, Faculty of Engineering and Science, Curtin University Malaysia, CDT 250, 98009 Miri, Sarawak Malaysia*
[2]*Mechanical Engineering Department, Abu Dhabi University, PO Box 59911, Abu Dhabi, UAE*
[3]*Department of Petroleum Engineering, Faculty of Engineering and Science, Curtin University Malaysia, CDT 250, 98009 Miri, Sarawak Malaysia*
[4]*Department of Mechanical Engineering, Universiti Teknologi PETRONAS, 32610, Seri Iskandar, Perak Malaysia*

†*Corresponding Author Email: sharulshambin.dol@adu.ac.ae*

ABSTRACT

The conventional method to promote mass, momentum and energy transport between fluid particles is to introduce a disturbance to the flow. An ultrasonic velocity profiler, UVP experiment was used to study the mean and fluctuating flow properties in the near wake of the rigid and flexible protruding surface in a water tunnel under the Reynolds number of 4000, 6000 and 8000. In the current study, circular finite cylinders (cantilevers) with various aspect ratios (AR = 10, 12, 14 and 16) and materials were used as the geometry of the rigid and protruding surface. The motion of the cylinder alters the fluid flow significantly. The increment of the wake region (~10% larger in the flexible cylinder compared to the rigid case, for AR = 16) is due to the weakening of the influence of downwash caused by the stream-wise deflection of the flexible cylinder. As a mean to quantify turbulence, the turbulent intensity, T_i, was studied. In general, the flexible cylinders show better capability in augmenting the turbulence than the rigid cylinder. The stream-wise turbulent intensity for AR = 16 and Re = 8000 can be as high as 97% for the flexible cylinder compared to only 26% for the rigid case. The normalized amplitude response graph, which records the cross-flow oscillation of the flexible cylinder was also analyzed. Under the same Reynolds number, the turbulence enhancement increases with the structural velocity. An organized oscillating motion is in favor of a higher performance of turbulence enhancement.

Keywords: Downwash; Flexible cylinder; Turbulent intensity; Ultrasonic velocity profiler; Wake region.

NOMENCLATURE.

AR	aspect ratio	T_i	turbulent intensity
D	cylinder diameter	U	free-stream velocity
EVA	Ethylene Vinyl Acetate	u'	turbulent velocity fluctuations
H	height of water tunnel	UVP	Ultrasonic Velocity Profiler
L	length of water tunnel	VIV	Vortex-Induced Vibration
Re	Reynolds number	W	width of water tunnel

1. INTRODUCTION

Basically, in order to achieve augmented turbulence, several mechanisms can be done through active or passive control. Active control uses external energy such as propeller, turbine, pump, nozzle jet or lobed mixer (e.g. a type of lobed shape design which can fit on the nozzle jet or be in part of the design to induce turbulence) to generate vortex while passive control generally utilizes the geometry (e.g. protruding surface) to affect the flow field in a fixed manner (Dol and Chan 2019; Mohan *et al.* 2015). A very commonly found device such as heat exchangers in various industries that aim to enhance the mixing and heat transfer, falls under the category of passive control device as the efficiency of heat exchangers is often heavily dependent on the configurations and shapes of the internal tubes. Passive control method is popular amongst many industries as it is cheaper to run, simpler to maintain

and easier to implement to suit their application needs. Despite that, the amount of turbulence generated is limited to the configurations of the geometry and the layout of the geometry.

However, there have been reports (Gupta and Uniyal 2012; Lin 2002) on the considerably low pressure recovery behind the protruding surface and it is inversely proportional to the turbulence enhancement. It is inevitable that the pressure losses in turbulence due to flow separation. As a result, the fluid loses energy in subsequent locations, thus the mean velocity is slowing down. The energy can be dissipated by viscous dissipation through the region where the boundary layer is formed. Apart from that, a portion of the kinetic energy in the oncoming flow can be "absorbed" by the protruding surface (the protruding surface which is like a rigid and stiff spring-like structure). The "absorbed" energy is then damped and wasted.

Since the low pressure recovery is inevitable, it is more important to increase the level of turbulence generated by the protruding surface. In addition, there is also a need to venture into innovative ideas to address the energy lost due to the rigid bluff body since the current approach of many researches is focusing on different configurations of rigid structures.

Inspired by the ingenious smart memory alloy (Aris *et al.* 2011) based protruding surface, the present work proposes to replace a conventional rigid protruding surface with a flexible protruding surface that has the ability to oscillate passively based on the incoming flow. Through the oscillation of the protruding flexible, the wasted energy "absorbed" by the rigid protruding surface is able to return to the flow by altering the flow dynamics. Therefore, the adoption of flexible protruding surface could eliminate the probability of pairing with an external energy supply (e.g. pumps).

There has been considerably large amount of efforts in studying three-dimensional flow in the past decade, in particular to the flow near the free end of a circular cylinder. Efforts are put into the free end due to the exclusively distinctive free end effects only a finite cylinder possess. Intrigued by the free end effects, researchers have focused intensively on the flow structure around the finite cylinder. As this research mainly study the flow dynamics around an oscillating finite cylinder, the focus will be on the flow dynamics due to vortex-induced vibration, therefore, the wake structure and the turbulence characteristics are the primary aspects to be reviewed even though there are very less studies on the flow dynamics aspect in the literature.

For the flow field around a finite cylinder, it is clear that the additional tip effects generated by the free end add a lot of complexity to the flow as it no longer consists of just Kármán vortices as witnessed by (Dol *et al.* 2020; Sumner 2013). Near the cylinder's free end exists a vortex pair that is counter-rotating in nature and curved downwards at the symmetry line. Below the free end region, the vortex is shed periodically, similarly to the classic Kármán vortex.

In other words, the wake becomes so complex that there exist two proposed models that describe the vortical structures at the free end. The complexity arises not because of the vortical structures near the free end itself; rather the interaction of these vortical structures that exist only in the three-dimensional flow.

Being intrigued with the flow complexities, some researchers started to perform qualitative research on the flow past cantilever cylinder. Park and Lee (2004) studied the flow visualization on cylinder with AR = 6 using a particle tracer method in a circulating water tunnel. They noticed that the trailing tip vortices are nearly symmetrical across the central plane in the near wake and have a similar size (see Fig. 1 (a)). It is noticeable that the separated shear layer moves towards the central region, forming large recirculating flow rotating in a clockwise direction (see Fig. 1 (b)). They attributed the downwash to the cause of trailing vortices. The irrotational flow at the downwash region affects vortex formation behind the cylinder and increases the vortex formation length. The vortices increase in size and shift downwards as they travel further downstream.
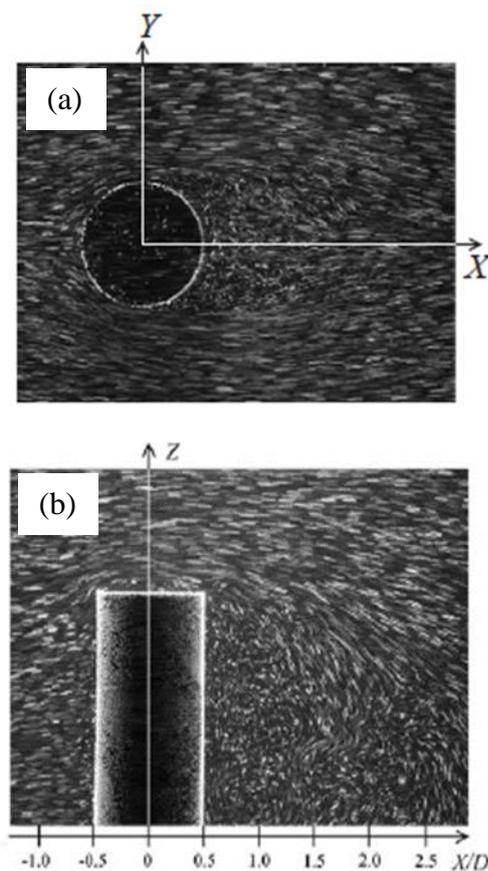

Fig. 1. (a) Top view of visualized flow in *x-y* plane (b) flow around finite cylinder at symmetrical plane. Adapted from (Park and Lee 2004).

It has been well-documented that the wake structure of the flow around the finite cylinder is different for

AR below and above some critical aspect ratios. The most notable change was the wake patterns where the downwash from the free end is dominant (the influence of downwash extends to the whole span of the finite cylinder until the base, leaving no room for upwash flow near the cylinder wall junction) for AR below the critical aspect ratio. Due to the strong downwash, the antisymmetric Kármán vortex shedding are also being suppressed. Okamoto (1991) referred this to the size of the recirculation region. The flow at the free end will reattach to the ground plane for small AR cylinders, resulting in the absence of upwash flow, if not very weak. When the upwash do exist for cylinder of AR above the critical aspect ratio, they originate near the ground plane and travel upwards towards the mid-height of the wake. When the tip effects seize at $3D$ to $4D$ from the tip (usually for cylinder of AR above the critical aspect ratio), the influence of downwash slowly decrease in strength from the free end to the base of the cylinder and reattachment of the end flow seize to occur. This observation is also consistent with the results from (Rostamy *et al.* 2012). Sumner *et al.* (2004) also noticed the existence of an upwash flow originates from the base of the cylinder, allowing the making of a second pair of counter-rotating vortices (also known as base vortex structures) within the wall boundary layer in addition to the counter-rotating pair of tip vortex structures near the free end for AR = 5, 7, and 9. Apart from that, a strong Kármán vortex shedding signal is detected, further confirms the existence of the antisymmetric Kármán vortex shedding for AR = 5, 7, and 9 and vice versa for AR = 3.

To date, there are less emphasis on the flow field behind a freely vibrating finite cylinder. This is especially true for experimental studies due to the feasibility and cost to investigate the flow properties. However, there are quite a few remarkable research studies (Kang and Jia 2013; Raghavan and Bernitsas 2011; Dahl *et al.* 2006; Jeon and Gharib 2001) on forced vibrating cylinders with either 1 DoF (either in-line or transverse to the flow only) or 2 DoF (both) on elastic supports and the focus was on the vortex structures in relation to the cylinder's structural properties. Though not as comprehensive, some of the authors did briefly discuss the flow structures caused by the vibrating cylinder.

Despite the major findings by some renowned researchers, they are all related to the elastically mounted cylinders which their both ends are fixed to the system's fixture, therefore no free end is exposed to the flow. This is because most of their work was motivated by the potential failure of marine engineering applications by VIV. As the experimental setup in this research work concerns flow past cantilever (with potential application in heat exchangers), the literature review might not be able to justify the condition of this research work in more exact manner. Moreover, the vibration of the flexible cylinder in this research work is not being restricted in any way, unlike the ones reviewed above. Nevertheless, there exists a few researchers who like to perform their investigations in a different approach.

The aim of this research is to investigate the flow dynamics in relation to the flexible protruding surface. The turbulence intensity was studied to quantify the turbulence characteristics in relations to the flow field at Reynolds numbers of 2500, 4000, 6000 and 8000. The ultrasonic velocity profiler measurements were divided into two categories: rigid cylinder cantilever and flexible cylinder cantilever. Flow in the lower subcritical Reynolds number regime $\sim x10^3$ is selected as the regime of interest as it is more compatible in most of the engineering applications.

2. MATERIALS AND METHODS

This chapter explains a detailed description of the experimental rig and apparatus used to perform the experiments. The cylinder models and its specification related to the freestream conditions are described here. Associated instrumentation such as the camera are also described in this section.

2.1 Water Tunnel

Experiments in the present study were conducted in circulating open channel water tunnel located at the Turbo Machine Laboratory, Universiti Teknologi PETRONAS that has dimensions of 1.2 m (*W*) x 1.2 m (*H*) x 3 m (*L*) and has a test section of 0.2 m (*W*) x 0.2 m (*H*) x 0.75 m (*L*) (see Fig. 2). The test section was fitted with tempered glass on one of the side wall, allowing complete view of the models for visualization purpose as well as visual inspection of the probe position. A poly-tube hexagonal honeycomb section was fitted upstream of the test section to straighten the flow reduce the turbulence intensity to no more than 7% at the region of interest of the test section depending on freestream velocity (see Fig. 3).

Fig. 2. Recirculating water channel.

All experiments conducted were at the middle of the test section where the boundary layers were expected to be fully developed. According to Fig. 3, the mean velocity profiles collapse onto a common point indicating a fully developed boundary layer was attained.

2.2 Ultrasonic Velocity Profiler

The velocity profile across the testing section was taken using a UVP (Ultrasonic Velocity Profiler), which was manufactured by MET-FLOW (Fig. 4). A low frequency transducer, 2 MHz, was used owing
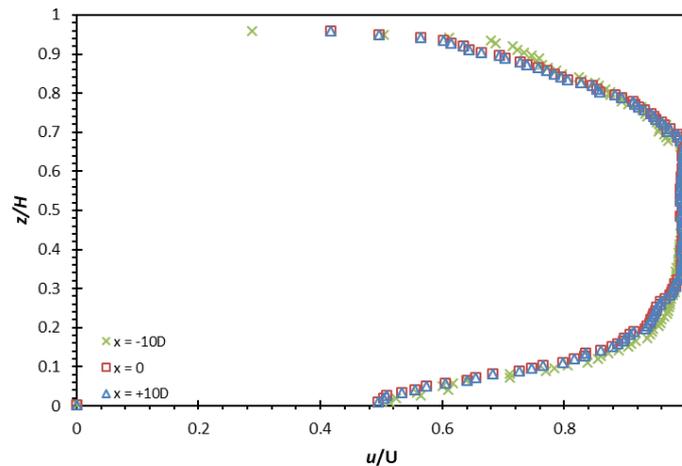
Fig. 3. Mean velocity profiles at three different locations at a freestream velocity of U = 0.49 m/s.
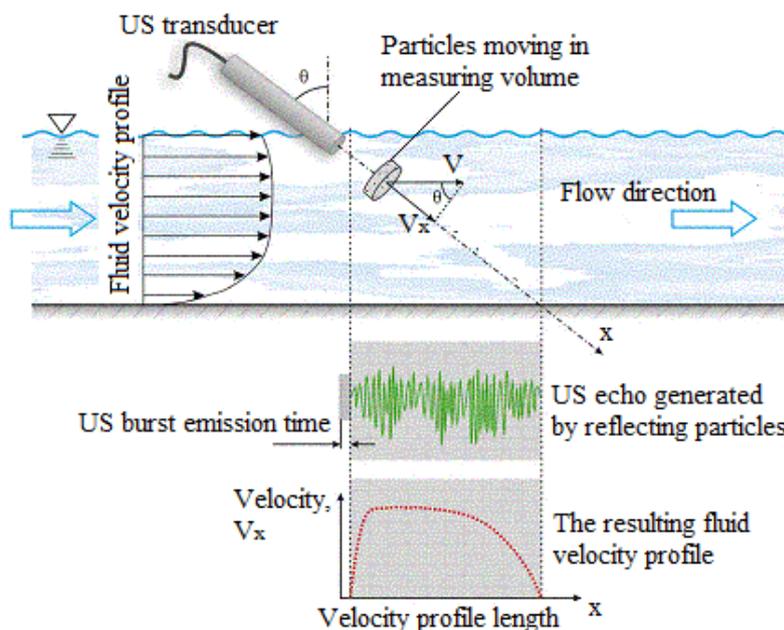

Fig. 4. Working principles of UVP monitor (METFLOW 2000).

to its ability to measuring long distance and large velocity. The 2 MHz transducer has a spatial resolution of 1.48 mm and depending on the parameters configuration; the velocity resolution can be as minimum as 0.36 mm/s and 193 mm/s at its maximum. The sampling period which it is capable to capture is 130 msec at its minimum and 0.2 msec at its maximum depending on parameters such as measured depth, velocity range, repetition and many more. The detailed working principle of the method is described in Takeda (1995).

During the event of one velocity component measurement, one transducer is sufficient owing to its linewise measuring capability. However, when measuring two or three velocity components, more than one transducers are needed (Yokoyama *et al.* 2004). They investigated the reliability of UVP in measuring one-dimensional and two-dimensional

flow in an open channel. They tested the accuracy of a single transducer in one-dimensional flow and also two-dimensional flow. They concluded that in the test of one-dimensional flow, the error was estimated to be 2.5% to about 7% depending on the incident angle of the transducer. The results show that smaller incident angle give a higher error. Nevertheless, it shows high accuracy of a single transducer in measuring one-dimensional flow.

The Doppler at large angles is more critical than it is at small angles in error estimation because the frequency shift becomes very small at large angles and the system sensitivity is reduced (Dol and Wong 2019; Dol *et al.* 2018). Nevertheless, three sets of measurements with different trajectory angle of 20° 30° and 40° were conducted in the investigation of the freestream quality and each set of trajectory angle was repeated three times. It was found from the mean

velocity profiles that the differences of the profiles measured from the trajectory angle of 20° and 30° were negligible, though the repeatability of trajectory angle of 30° was better. As a result of that, trajectory angle of 30° was used. A 256 pulse of repetitions was selected throughout the experiments (one velocity profile is determined after 256 repetitions whereby the repetition represents the number of samples the echo signals reflected which the system uses it to reconstruct the Doppler frequency correctly). A sampling rate of 1 kHz was used in obtaining 3000 samples of the profiles. The spatial resolution is 1.47 mm.

2.3 Finite and Flexible Circular Cylinders

Two smooth aluminum circular models with a diameter $D = 13.0 \pm 0.5$ mm and 11.0 ± 0.5 mm and AR = 10 and 16 (see Fig. 5) were used. Each cylinder has a flat and sharp edge. The surface of all the experimental models was assumed to be smooth and no surface roughness manipulation was treated as skin friction in the laminar boundary layer is insignificant. The blockage ratio was at most 4.8%, which is still well acceptable within the prescribed range for cylinder flows (Dol *et al.* 2014). The measurements were done at the following Reynolds numbers based on the diameter of the cylinders, *Re* = 4000, 6000 and 8000.

Fig. 5. Two aluminium cylinders with AR = 10 and 16.

As for the experiments of finite flexible circular cylinders, it is separated into two categories by the choice of materials – metal and polymer. Under the category of metal, aluminum cylinder and carbon steel cylinder were used, whereas Ethylene vinyl acetate, EVA cylinder was chosen for the category of polymer.

The diameter of the aluminum and carbon steel cylinder was $D = 3.0 \pm 0.5$ mm (see Fig. 6). Two AR = 50 and 54 of the aluminum and carbon steel cylinder were investigated in these experiments. The intentionally large AR was chosen for two reasons. First, the stiffness of metal is significantly higher

than that of polymer. Thus, in order for the cylinder to experience vibration induced by the different pressures caused by the vortex shedding, the diameter and the length must be kept small and long. Second, the height was physically limited by the water tunnel dimensions. On the other hand, four EVA cylinders with diameter $D = 11.0 \pm 0.5$ mm and AR = 10, 12, 14, and 16 (see Fig. 7) were used in these experiments. The cylinder was located at the same position as the finite rigid circular cylinder (350 mm from the leading edge). The blockage ratio was at most 1.2% for metal group models and 4.8% for polymer group models. The measurements were done at the following Reynolds numbers based on the diameter of the cylinders, *Re* = 2500 (metal group) and 4000, 6000 and 8000 (polymer group). A Reynolds number of *Re* = 2500 was selected for the metal group flexible cylinder because it was limited by the maximum freestream velocity available due to a very high *U* that was needed to achieve the same *Re* as the polymer group cylinder.

Fig. 6. Aluminium and carbon steel cylinders with AR = 50 and 54.

2.4 Camera and Image Processing

In order to visualize the oscillations by flexible cylinder inside the recirculating water tunnel, a Canon Eos 60D camera was used. The camera is capable of recording 60 fps at 1280 x 720 pixels. The camera lens was mounted directly above the flexible cylinder where the oscillating motions were recorded and the distance between the lens and the cylinder's free end were kept constant. It is important that the lens was perfectly aligned to the cylinder's free end so that the light wave is approaching the water in a direction which is perpendicular to the water surface since theoretically the light does not refract at the normal line. A 5 mm grid that was true to scale was marked on the end plate at the location where the cylinder was installed.

Table 1 Summary of uncertainty estimation in the freestream parameters and experimental model dimensions

Parameter	Uncertainty (%)
Freestream Density, ρ	± 1.17
Freestream Kinematic Viscosity, V	± 1.16
Freestream Velocity, U	± 3.64
Cylinder Diameter, D	± 0.38
Cylinder Length, L	± 0.76
Reynolds Number, Re	± 4.41

Fig. 7. Four EVA cylinders with AR = 10, 12, 14 and 16.

The video was analysed by using a motion analysis software, Photon FASTCAM Analysis version 1.3.2.0. The motion software has an automatic tracking feature which identifies the pixel of the point of interest. Users can key-in input the actual dimension of any objects in the video and the software will automatically calculate the distance corresponded to a single pixel.

2.5 Uncertainty Analysis

The uncertainty estimation for the different parameters are calculated based on the Coleman and Steele (1999) approach at a 90% confidence level. Based on the approach, the summary of the uncertainty estimation in the freestream parameters and experimental model dimensions are presented in Table 1.

3.   RESULTS AND DISCUSSIONS

This section presents the results of the rigid finite circular cylinders and flexible finite circular cylinders investigated under Reynolds number of 4000, 6000 and 8000. As this section mainly aims to identify the difference in the wake structure between rigid and flexible finite circular cylinders, only cylinders of AR = 10 and 16 will be discussed.

The study of velocity profiles might be the easiest way to comprehend the size of the wake region between the rigid and flexible cylinders. It provides information such as the direction the mean flow is travelling and also the wake region. The information on where the mean flow is traveling is extremely important as the vortices generated from the free end of the cylinder will follow the path of the mean flow. The time-averaged stream-wise ($\bar{u}/U$) and wall-normal ($\bar{w}/U$) velocity profile of rigid and flexible finite cylinders of AR = 10 and 16 at Re = 4000, 6000 and 8000 have been reported comprehensively in our previous publication by Yong *et al.* (2017).

Yong *et al.* (2017) reported that the flow behind the rigid cylinder at $x/D \leq 3$ is brought downwards to the floor along the wake centerline. The $\bar{u}$ component velocity slowly gain velocity until it finally dominates the $\bar{w}$ component velocity at circa $x/D \geq$ 3. The phenomenon of the flow convected downwards is called downwash. Since the vortex mainly follows the path of the mean flow, in the case of the rigid cylinder, most of the vortices generated are transported downwards along the cylinder span rather than transported downstream due to the influence of the downwash flow that cause the tip effects.

As the influence of downwash phenomena is very negligible behind a flexible cylinder, the tip vortex generated can be transported downstream more effectively without being down-washed towards the ground and dissipated. Thus, the effective area of which the turbulent activities happen improves considerably. The average wake region in accordance to the rigid and flexible cylinders in different AR and Re are presented in Table 2. It is with substantial evidence that the wake region increment is achieved through the use of flexible cylinder. However, there are two additional

Table 2 Average wake region behind the rigid and flexible cylinders at different conditions

		Average wake region		
AR	Re	Rigid Cylinder	Flexible Cylinder	Increment (%)
10	4000	~ 7.0 *D*	~ 7.0 *D*	0
	6000	~ 7.0 *D*	~ 7.7 *D*	~ 10.00
	8000	~ 7.2 *D*	~ 8.0 *D*	~ 11.10
16	4000	~ 13.0 *D*	~ 14.4 *D*	~ 10.77
	6000	~ 13.1 *D*	~ 14.2 *D*	~ 8.40
	8000	~ 13.0 *D*	~ 14.4 *D*	~ 10.77

phenomena that is associated with the flexible cylinder – deflection in the stream-wise direction and oscillation traverse to the flow. Therefore, the roles of these phenomena are examined in the subsequent discussion.

As an effort to provide substantial evidence that shows the different wake region by the rigid and flexible cylinder, a separate set of experiment that utilizes the high-speed camera capability to capture the flow pattern behind the rigid and flexible cylinders was conducted. A rigid cylinder of AR = 10 and a flexible EVA cylinder of AR = 16 that were operating at *Re* = 3500 were being recorded with tracers.

The wake behind the rigid cylinder shows strong influence of the downwash, especially below the free end. A circular region below the free end is spotted, which brings the flow downwards to the ground, also confirmed by Park and Lee (2000). On the other hand, the most notable feature of the flow behind the flexible cylinder is the absence of downwash and tip effects, as shown in Fig. 8. Due to the absence of the downwash flow, no strong influence of downwash can be seen in the near wake of the cylinder. The tracer is transported downstream instead of downwards. Hence, the vortices associated with the flow can be transported and prolonged downstream, expanding the effectiveness of turbulence region. The wake region is seen on the same height as the free end of the cylinder, proving the effectiveness of the flexible cylinder in increasing the wake region.

3.1 Roles of Deflection and Oscillation of the Flexible Cylinder on the Wake Region

The same phenomenon had been discovered by (Park and Lee 2000; Roh and Park 2003; Okamoto and Yagita 1973) in their experimental results and concluded the downwash effect is the main contributor to this phenomenon. The vortex generated is therefore drawn to the floor instead of transported downstream, making the wake size smaller in the case of rigid cylinders, regardless of AR. The absence of downwash for the flexible cylinders on the other hand, suggests that the vortices generated at the free end can be transported downstream once it has received enough energy and detach itself from the boundary layer or under circumstances that it is forced to detach due to the interference of the structural motion that is vibrating (Dol *et al.* 2014). As a result of that, the wake region
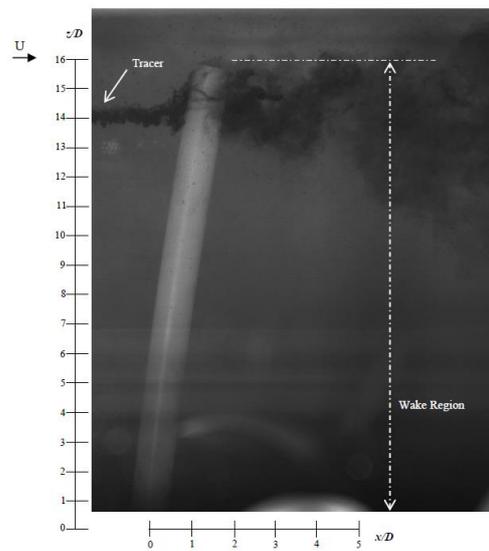
can be larger than that behind the rigid cylinders.

Fig. 8. Flow visualization of flexible cylinder of AR =16 and *Re* = 3500.

It is because of the elastic property of the flexible cylinders possess, the additional two phenomena emerge – a) deflection and b) oscillation. With reference to the Fig. 9, the oscillation of flexible cylinders comprises the oscillating motion, oscillating frequency and the oscillating amplitude. When put into comparison of the wake structure and its respective cylinder's oscillation response, it can be observed that the wake structure from the velocity profiles of the flexible cylinders under any condition are irrelevant of the oscillation response because the oscillating motion, frequency and amplitude are distinctive at each *Re*; while the wake region behind the flexible cylinders under all *Re* behaves quite similar.

The stream-wise deflection on the other hand though, has its effect on the downwash and subsequently the wake region behind the cylinder. The degree of deflection, as can be seen from Fig. 10, are different. In comparison to its respective velocity profiles in Yong *et al.* (2017), presence of downwash can be discerned from the static cylinders (no deflection) associated with it. Apart from that, the increase in

wake region is also seen associate with higher stream-wise deflection. From Table 2, there is no increment in the wake region because the flexible EVA cylinder of AR = 10 at Re = 4000 was not deflected at all. As the Re is increased, the deflection of the flexible EVA cylinder of AR = 10 increases; hence, the increment in the wake region as well.
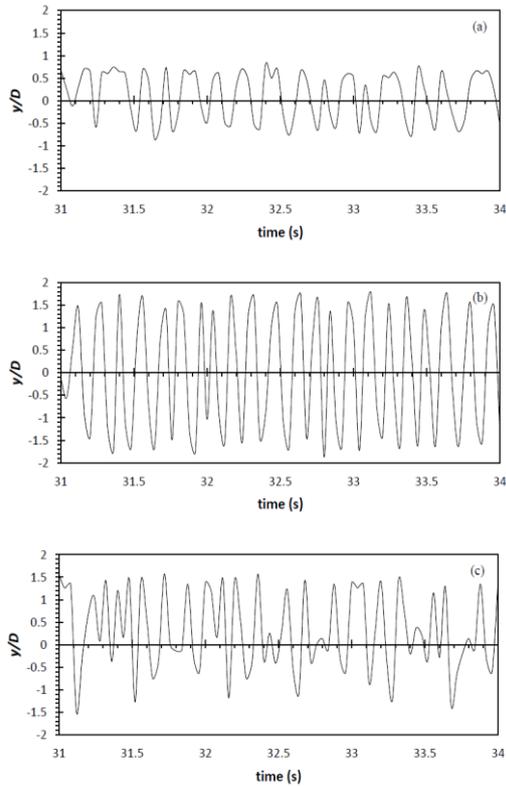

Fig. 9. Oscillation of flexible cylinder of AR = 16; (a) Re = 4000 (b) Re = 6000 (c) Re = 8000.

It would seem that the greater in deflection of the cylinder, the effect of downwash is less pronounced and therefore the velocity of $\bar{u}$ component flow behind the cylinder at the same location as cylinders with less deflection is recovering quicker towards the freestream velocity (Yong *et al.* 2017). It has been demonstrated by (Kawamura *et al.* 1984; Taniguchi *et al.* 1981) that there exists a large pressure drop (higher pressure in front of the cylinder and lower pressure behind the cylinder) for the rigid finite cylinder that leads to the downwash behind the cylinder. Since the velocity profile distributions of the flexible cylinder show that downwash is weaken or diminished, the pressure drop behavior could have been altered for the flexible cylinder. The pressure drop could have been lessen for the downwash phenomenon to be weaken or the pressure distribution around the deflected cylinder could be have been altered. The turbulence characteristics of the flexible cylinder will be examined and discussed through the turbulence intensity of the flow field to further solidify the improvement brought by the flexible cylinder over rigid cylinder.
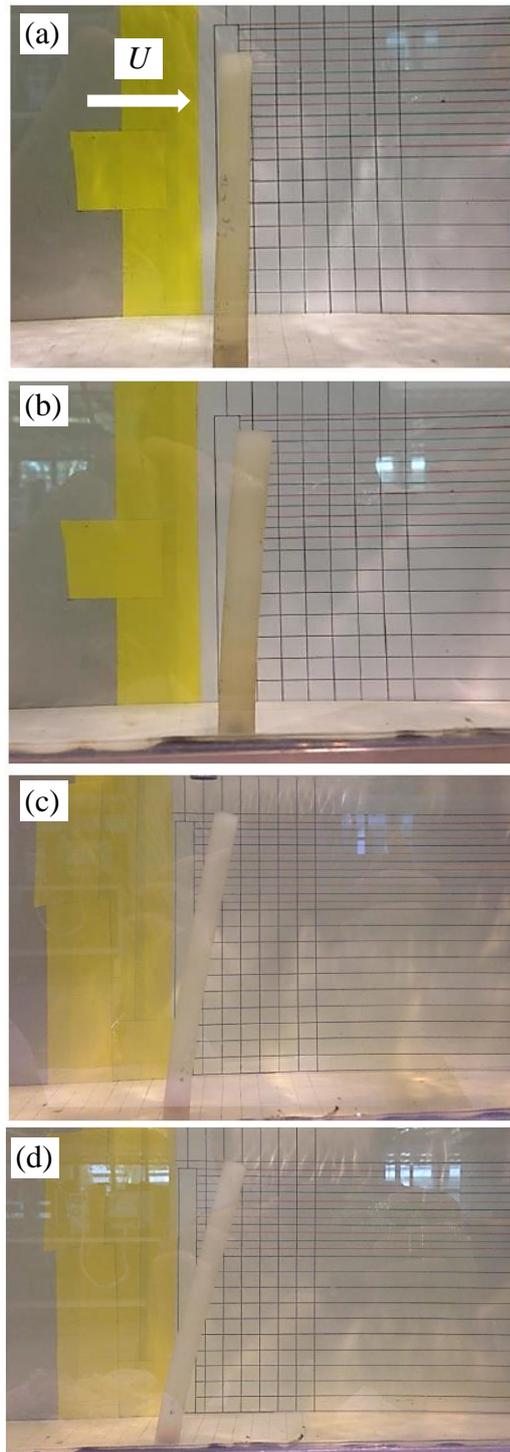

Fig. 10. Flexible cylinder showing various degrees of bending; (a) AR = 10, Re = 6000 (b) AR= 10, Re = 8000 (c) AR = 16, Re = 4000 (d) AR = 16, Re = 6000 and 8000.

3.2 Turbulence Intensity Distribution

Turbulence intensity is perhaps the most direct indication in evaluating the level of turbulence in the flow that examines the fluctuations about the mean. As the turbulent motions associated with the eddies are random, the study of turbulence intensity is able to characterize how a random variable is distributed
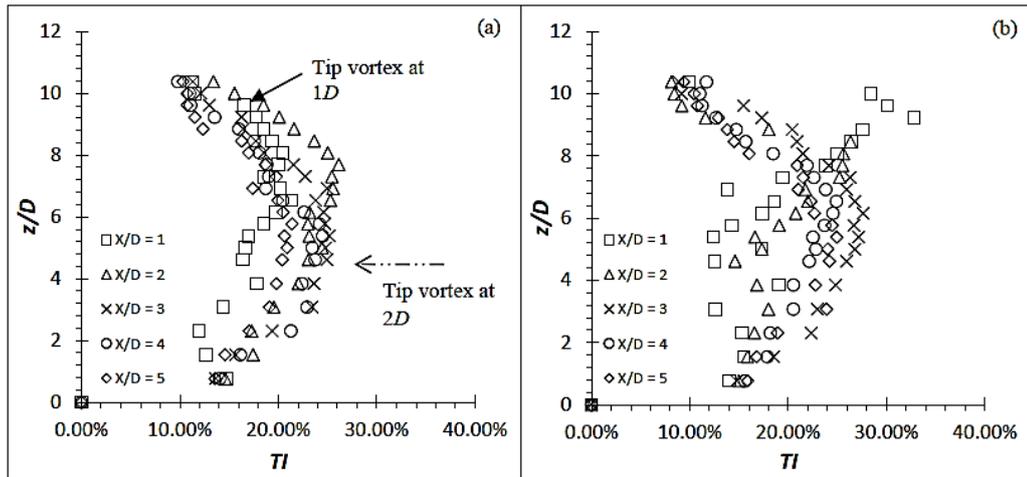
Fig. 11. T_i **distribution for rigid cylinder of AR = 10 at** *Re* **= 4000: (a)** *u'/U* **(b)** *w'/U*.

about the mean flow. The equation of the turbulence intensity can be written as:

$$T_i = \frac{u'}{U} \tag{1}$$

where u' is the rms of the turbulent velocity fluctuations and U is the averaged mean velocity. A higher turbulence intensity indicates a higher level of turbulence in the flow. Therefore, by examining the localized turbulence intensity in the near wake of the rigid and flexible cylinder of AR = 10 and 16 in accordance with its deflection and oscillation motions, it is hoped that the reason behind the changes in the localized turbulence intensity between the rigid and flexible cylinder could be answered.

The distributions of the stream-wise turbulence intensity (u'/U) and the wall-normal turbulence intensity (w'/U) of rigid cylinder of AR = 10 at *Re* = 4000 in the wake centerline ($y/D = 0$) are shown in Fig. 11. As seen from Fig. 11 (a), the localized maximum turbulence intensity (u'_{max}/U) ≈ 26% can be seen located at $z/D ≈ 8$ of the cylinder at $x/D = 2$; consistent with the existence of the tip vortex where it has a greater strength as witnessed by (Rostamy *et al.* 2012; Park and Lee 2004) in their experiments where the higher turbulence intensity coincides with the tip vortex. The tip vortex at $x/D = 1$, slightly at a smaller value is extended into the region of the downwash flow within the near wake and hence, the local (u'_{max}/U) is found to be at $z/D ≈ 7$ and 8 (see the long dashed double dot arrow marked at Fig. 11 (a) for $x/D = 3$).

Below the region, the influence of tip vortex is becoming weaker that it can no longer suppress the formation of Kármán vortex, therefore, the regular Kármán vortex is present below the tip vortex and can be represented by the considerable weaker turbulence intensity value (Rostamy *et al.* 2012). It is however important to note that the freestream turbulence intensity was at circa 11%, so the increment of the turbulence intensity at the tip is only a mere approximate 15%. The phenomenon of (u'_{max}/U) near the mid-height span can also be seen

through findings from (Afgan *et al.* 2007; Park and Lee 2004; Sumner *et al.* 2004; Park and Lee 2000), which they regarded that as the region that are bounded on the four corners by the tip and base vortices. As this region is the focal point where the vortex structures, vortex street, downwash and upwash meet, it is highly interactive.

The (w'/U) also show a concentrated region at the near mid-height at $x/D ≈ 3$ which also corresponds to the interaction of upwash and downwash. As the higher turbulence intensities region for both components move downwards as x/D increases, it can be said that vortex generated does indeed being downwashed.

Figure 12 shows the distributions of the (u'/U) and the (w'/U) of rigid cylinder of *AR* = 16 at *Re* = 4000 in the wake centerline ($y/D = 0$). Similar to what is found in cylinder of AR = 10 at *Re* = 4000, the (u'_{max}/U) of AR = 16 at circa 29% can be seen located at $z/D ≈ 13$ where the tip vortex is being downwashed and transported downwards. It shows that at the span roughly below 4*D* from the free end, the regular Kármán vortex shedding becomes dominant. There is an overall increment of turbulence intensity as the AR increases (as shown in Figs. 11 and 12).

The distributions of the stream-wise turbulence intensity (u'/U) and the wall-normal turbulence intensity (w'/U) of flexible cylinder of AR = 10 and 16 at *Re* = 4000, 6000 and 8000 in the wake centerline ($y/D = 0$) are shown in Fig. 13 to Fig. 18. With reference to the (u'/U) distribution of the rigid cylinders, which shows no major changes at different AR; the (u'/U) distribution of flexible cylinders (see Fig. 15 (a) to Fig. 18 (a)) shows the upwards shifting of the local (u'_{max}/U) compared to the rigid cylinder. While the rigid cylinder has roughly (u'_{max}/U) at $z/D ≈$ AR - 3*D* to 4*D*, the flexible cylinder has approximately (u'_{max}/U) at $z/D ≈$ AR - 1*D* to 2*D* at $x/D = 3$, 4, and 5 subjecting to the order of the magnitude of deflection; roughly equivalent to the deflected height of flexible cylinder. This indicates
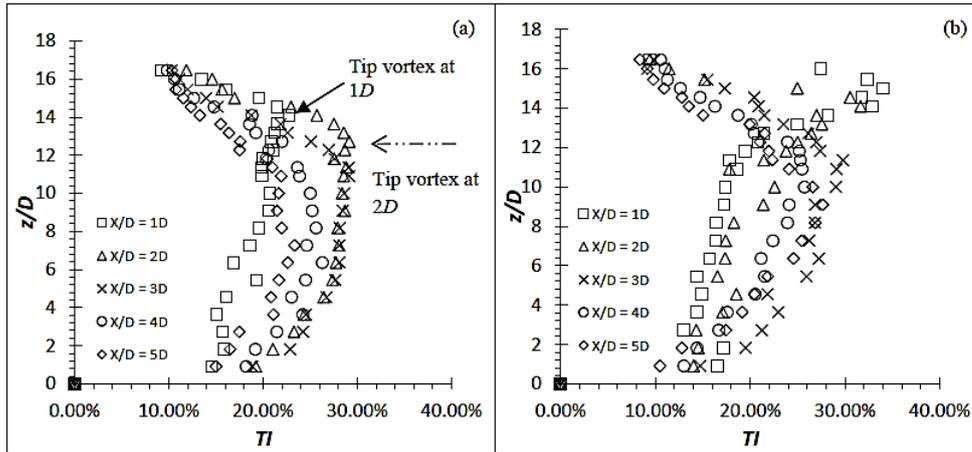
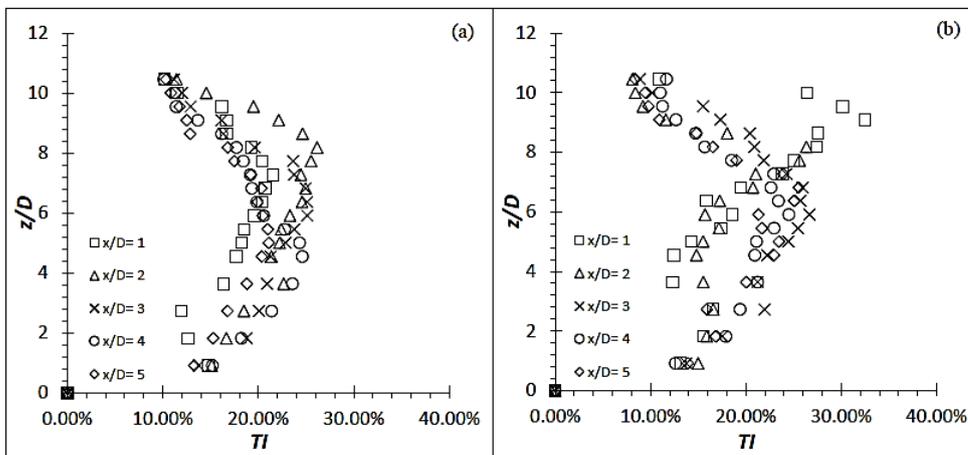**Fig. 12.** T_i distribution for rigid cylinder of AR = 16 at *Re* = 4000: (a) *u'*/*U* (b) *w'*/*U*.

Fig. 13. T_i distribution for flexible cylinder of AR = 10 at *Re* = 4000: (a) *u'*/*U* (b) *w'*/*U*.
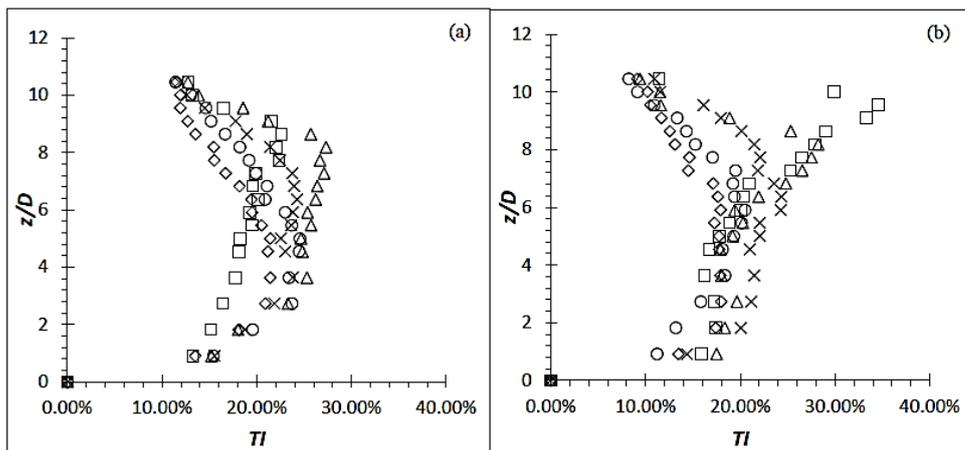

Fig. 14. T_i distribution for flexible cylinder of AR = 10 at *Re* = 6000: (a) *u'*/*U* (b) *w'*/*U*.

that the tip vortex generated is not being downwashed as the vortex follows the path of the bulk flow.

The cylinder of AR = 10 at *Re* = 4000 and 6000 do

not experience major increment as it behaves nearly the same as the rigid cylinder of the same condition. This could be due to the fact that the cylinder at *Re* = 4000 and 6000 do not oscillate and deflect, which acts like a rigid cylinder. The cylinder at *Re* = 8000 has spotted a slight increment.
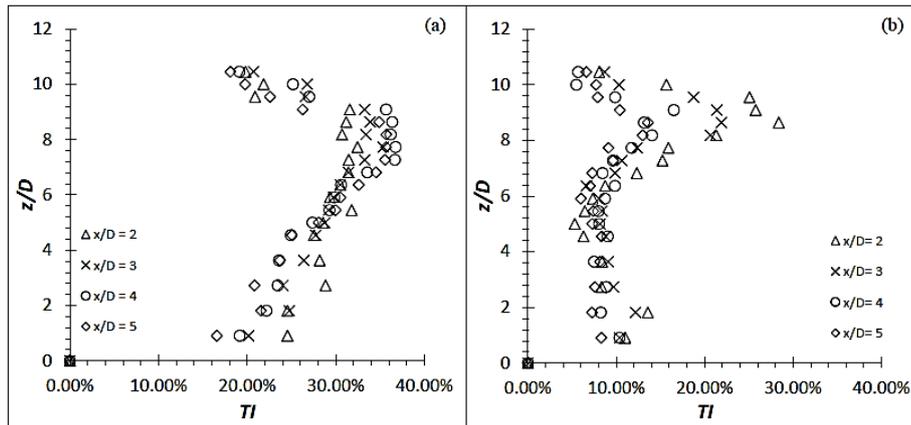
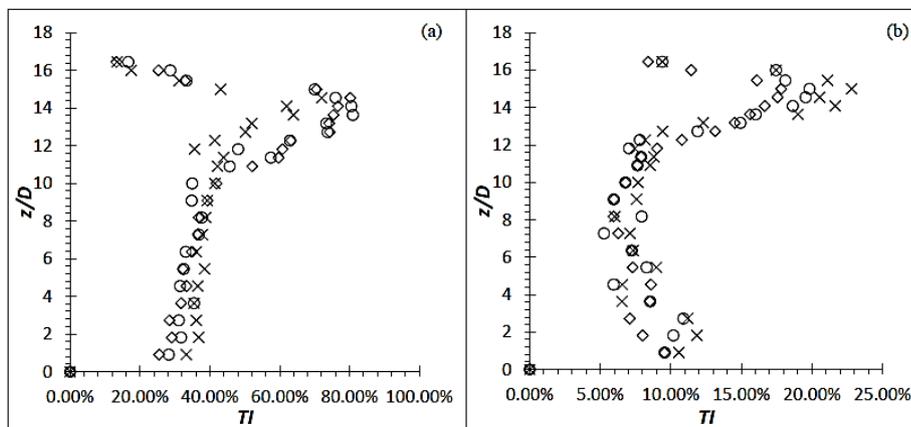**Fig. 15.** T_i distribution for flexible cylinder of AR = 10 at *Re* = 8000: (a) *u'/U* (b) *w'/U*.

Fig. 16. T_i distribution for flexible cylinder of AR = 16 at *Re* = 4000: (a) *u'/U* (b) *w'/U*.
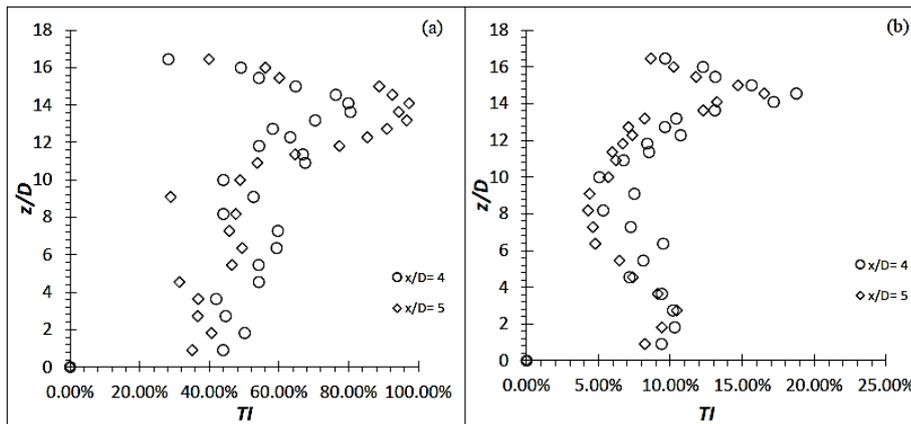

Fig. 17. T_i distribution for flexible cylinder of AR = 16 at *Re* = 6000: (a) *u'/U* (b) *w'/U*.

According to the (*u'/U*) distribution of the rigid and flexible cylinders, increase in magnitude of the (*u'/U*) of flexible cylinders can also be discerned. It is the increment in the magnitude that shows the potential of flexible cylinders in enhancing turbulence in the flow. The (u'_{max}/U) of the flexible cylinder of AR = 10 and 16, which is approximately at *z/D* ≈ AR - 2*D*, ranged from ~37% to 97% from AR = 10 at *Re* = 8000 to AR = 16 at *Re* = 8000. It is a huge increment over the rigid cylinders which is at a mere 26% of AR = 10 at *Re* = 4000.

Surprisingly, according to Fig. 17 (a) and Fig. 18 (a), the local (u'_{max}/U) for *Re* = 8000 is lower than that of 6000. However, this could be attributed to the
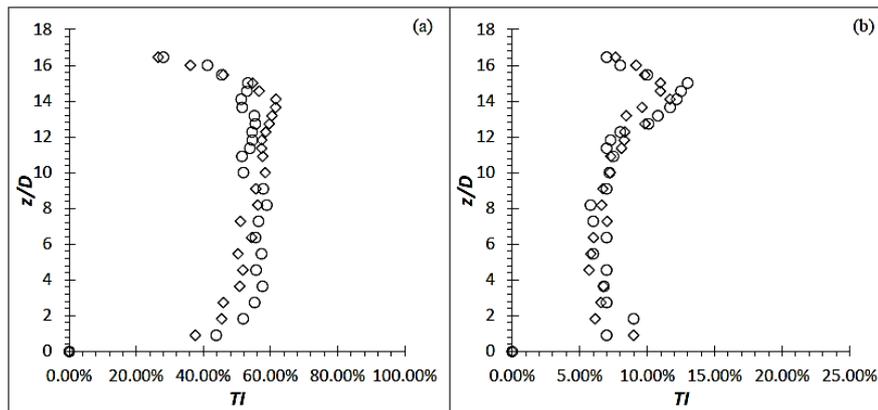
Fig. 18. T_i distribution for flexible cylinder of AR = 16 at *Re* = 8000: (a) *u'/U* (b) *w'/U*.

disorganized oscillating motion and also the oscillation that happens off-axis (see Fig. 9 (c)) for *Re* = 8000. The word "disorganized" in this context means that the oscillation of the cylinder does not follow the typical sinusoidal wave where the frequency and amplitude become slow/low at few cycles and the existence of double or triple crests and troughs (see Fig. 9 (b) and (c) for illustration and comparison). Nevertheless, the overall turbulence intensity distribution of the flexible cylinders shows considerable improvement over the rigid cylinders in promoting turbulent activities in the flow (Dol *et al.* 2019).

The (*w'/U*) on the other hand, shows a general reduction in the magnitude at the mid-span of the flexible cylinders. The turbulence intensity near the free end of the flexible cylinders shows decrease in the magnitude from circa 32% for the rigid cylinders to 13% at the lowest for the flexible cylinders. The fluid particle is therefore not active in the *w*-component. The reason could be because it has no downwash flow behind the cylinder and thus the fluctuation in *w* component is not active. Nevertheless, the (*u'/U*) of the flexible cylinder has seen increasing so significantly (in the range of 37% to 97%) over the rigid cylinder, though a slight reduction in the (*w'/U*), it still shows vast improvement over the rigid cylinder.

4. CONCLUSION

In general, it is seen that the wake region behind the flexible cylinder is greater than the rigid cylinder in agreement with the earlier findings. An increase in the wake region indicates that the effective region of the turbulence activities is increased. The turbulence intensity produced by the all the EVA and aluminum flexible cylinder experienced an increment over the rigid cylinder. The carbon steel flexible cylinder however, did not experience any gain in value of the turbulence intensity as they behaved exactly like a rigid cylinder. Based on the results, it is concluded that the cause of the augmented turbulence intensity produced by the flexible cylinder is due to the oscillation of the flexible cylinder. Three oscillating parameters namely oscillating amplitude, oscillating

frequency and oscillating motion are identified to have altered the turbulence intensity.

REFERENCES

Afgan, I., C. Moulinec, R. Prosser and D. Laurence (2007). Large eddy simulation of turbulent flow for wall mounted cantilever cylinders of aspect ratio 6 and 10. *International Journal of Heat and Fluid Flow* 28(4), 561-574.

Aris, M. S., I. Owen and C. J. Sutcliffe (2011). The development of active vortex generators from shape memory alloys for the convective cooling of heated surfaces. *International Journal of Heat and Mass Transfer* 54(15), 3566-3574.

Coleman, H. W. and W. G. Steele (1999). *Experimentation and Uncertainty Analysis for Engineers.* 2nd Edition, Wiley, New York.

Dahl, J. M., F. S. Hover and M. S. Triantafyllou (2006). Two-degree-of-freedom vortex-induced vibrations using a force assisted apparatus. *Journal of Fluids and Structures* 22(6), 807-818.

Dol, S. S. and H. B. Chan (2019). Fluid-Structural Interaction Simulation of Vortices behind a Flexible Vortex Generator. *2019 8th International Conference on Modeling Simulation and Applied Optimization (ICMSAO)* pp. 1-5. IEEE.

Dol, S. S., H. B. Chan, S. K. Wee and K. Perumal (2020). The effects of flexible vortex generator on the wake structures for improving

turbulence. In *IOP Conference Series: Materials Science and Engineering*, vol. 715, no. 1, p. 012070. IOP Publishing.

Dol, S. S., M. M. Salek and R. J. Martinuzzi (2014). Effects of pulsation to the mean field and vortex development in a backward-facing step flow. *Journal of Fluids Engineering* 136(1), 011001.

Dol, S. S., S. K. Wee, H. B. Chan and K. Perumal (2019). Turbulence Characteristics behind a Flexible Vortex Generator, *WSEAS TRANSACTIONS ON FLUID MECHANICS* 14, 1-7.

Dol, S. S. and S. F. Wong (2019). Turbulence Characteristics Study of the Emulsified Flow. *WSEAS TRANSACTIONS ON HEAT AND MASS TRANSFER* 14, 45-50.

Dol, S. S., S. F. Wong, S. K. Wee and J. S. Lim (2018). Experimental Study on the Effects of Water-in-oil Emulsions to Wall Shear Stress in the Pipeline Flow. *Journal of Applied Fluid Mechanics* 11(5), 1309-1319.

Gupta, A., and M. Uniyal (2012). Review of heat transfer augmentation through different passive intensifier methods. *IOSR Journal of Mechanical and Civil Engineering (IOSRJMCE) ISSN,* 2278-1684.

Jeon, D. and M. Gharib (2001). On circular cylinders undergoing two-degree-of-freedom forced motions. *Journal of Fluids and Structures* 15(3), 533-541.

Kang, Z. and L. Jia (2013). An experiment study of a cylinder's two degree of freedom VIV trajectories. *Ocean Engineering* 70, 129-140.

Kawamura, T., M. Hiwada, T. Hibino, I. Mabuchi and M. Kumada (1984). Flow around a Finite Circular Cylinder on a Flat Plate: Cylinder height greater than turbulent boundary layer thickness. *Bulletin of JSME* 27(232), 2142-2151.

Lin, J. C. (2002). Review of research on low-profile vortex generators to control boundary-layer separation. *Progress in Aerospace Sciences* 38(4), 389-420.

Metflow (2000). *UVP Monitor – Model UVP-XW, Users guide..* Met-flow SA, Lausanne, Switzerland: s.n.

Mohan, N. D., D. Greenblatt, C. N. Nayeri, C. O. Paschereit and N. R. Panchapakesan (2015). Vortex-enhanced mixing through active and passive flow control methods. *Experiments in Fluids* 56(3), 1-16.

Okamoto, S. (1991). Flow Past Circular-Cylinder of Finite Length Placed On Ground Plane.

Transactions of the Japan Society for Aeronautical and Space Sciences 33(102), 234-246.

Okamoto, T. and M. Yagita (1973). The experimental investigation on the flow past a circular cylinder of finite length placed normal to the plane surface in a uniform stream. *Bulletin of JSME* 16(95), 805-814.

Park, C. W. and S. J. Lee (2000). Free end effects on the near wake flow structure behind a finite circular cylinder. *Journal of Wind Engineering and Industrial Aerodynamics* 88(2), 231-246.

Park, C. W. and S. J. Lee (2004). Effects of free-end corner shape on flow structure around a finite cylinder. *Journal of Fluids and Structures* 19(2), 141-158.

Raghavan, K. and M. M. Bernitsas (2011). Experimental investigation of Reynolds number effect on vortex induced vibration of rigid circular cylinder on elastic supports. *Ocean Engineering* 38(5), 719-731.

Roh, S. and S. Park (2003). Vortical flow over the free end surface of a finite circular cylinder mounted on a flat plate. *Experiments in Fluids* 34(1), 63-67.

Rostamy, N., D. Sumner, D. J. Bergstrom and J. D. Bugg (2012). Local flow field of a surface-mounted finite circular cylinder. *Journal of Fluids and Structures* 34, 105-122.

Sumner, D. (2013). Flow above the free end of a surface-mounted finite-height circular cylinder: a review. *Journal of Fluids and Structures* 43, 41-63.

Sumner, D., J. L. Heseltine and O. J. P. Dansereau (2004). Wake structure of a finite circular cylinder of small aspect ratio. *Experiments in Fluids* 37(5), 720-730.

Takeda, Y. (1995). Velocity profile measurement by ultrasonic Doppler method. *Experimental Thermal and Fluid Science* 10(4), 444-453.

Taniguchi, S., H. Sakamoto and M. Arie (1981). Flow around circular cylinders of finite height placed vertically in turbulent boundary layers. *Bulletin of JSME*, 24(187) 37-44.

Yokoyama, K., N. Kashiwaguma, T. Okubo and Y. Takeda (2004). Flow measurement in an open channel by UVP. *Proceedings, ISUD 4*, 204-210.

Yong, T. H., H. B. Chan, S. S. Dol, S. K. Wee and P. Kumar (2017, June). The flow dynamics behind a flexible finite cylinder as a flexible agitator. In *IOP Conference Series: Materials Science and Engineering* 206(1), p. 012033). IOP Publishing.